As originally published in the IPC APEX EXPO Proceedings.

Investigation of Pad Cratering in Large Flip-Chip BGA using Acoustic Emission

Anurag Bansal, Cherif Guirguis and Kuo-Chuan Liu
Cisco Systems, Inc.,
San Jose, CA
anurbans@cisco.com

Abstract
Electronics assemblies with large flip-chip BGA packages can be prone to either pad cratering or brittle intermetallic (IMC) failures under excessive PCB bending. Pad cratering cracks are not detected by electrical testing or non-destructive inspection methods, yet they pose a long term reliability risk since the cracks may propagate under subsequent loads to cause electrical failure. Since the initiation of pad cratering does not result in an instantaneous electrical signature, detecting the onset of this failure has been challenging. An acoustic emission methodology was recently developed by the authors to detect the onset of pad cratering [1, 2]. The instantaneous release of elastic energy associated with the initiation of an internal crack, i.e., Acoustic Emission (AE), can be monitored to accurately determine the onset of both pad cratering and brittle intermetallic (IMC) failures.

In this study, the AE technique is used to systematically investigate pad cratering in a daisy chain 40 x 40 mm Flip-Chip BGA (FCBGA) package with lead-free SAC305 solder balls and 1 mm ball pitch. AE sensors have been attached to a four-point bend test vehicle to determine the onset of either pad cratering or brittle IMC failures. A two-dimensional AE source location method has been used to determine the planar location of failures on the test board. The test matrix is designed to investigate the effects of normal or diagonal strain orientation, NSMD or SMD PCB pads, and single or multiple reflow cycles. Physical failure analysis has been performed to correlate the test results with failure modes.

Introduction
Pad cratering refers to the formation of fine cohesive cracks under BGA pads in organic substrates or PCB laminate materials (Figure 1). These cracks have been known to occur under excessive mechanical bending or shock loads that may be applied in PCBA assembly, test, and handling operations [3-6]. Studies have also shown that pad cratering can occur under high thermal strains such as those experienced during SMT reflow processing, thermal cycling with a wide temperature range or thermal shock conditions [7]. The concern for pad cratering has been elevated with the increased use of large body size FCBGA components and fine pitch pad geometries. Furthermore, in comparison with the conventional tin-lead solder alloys, studies have shown that the risk for pad cratering is higher in lead-free assemblies. This is because the stress concentration under BGA pads is higher with the use of the significantly stiffer and more brittle Sn-Ag-Cu (SAC) based alloys, and also due to the use of higher reflow temperatures in assembly [4]. In addition, the Phenolic cured laminate materials compatible with lead-free assembly are more brittle than Dicy cured laminates used in conventional tin-lead assembly processes [8].

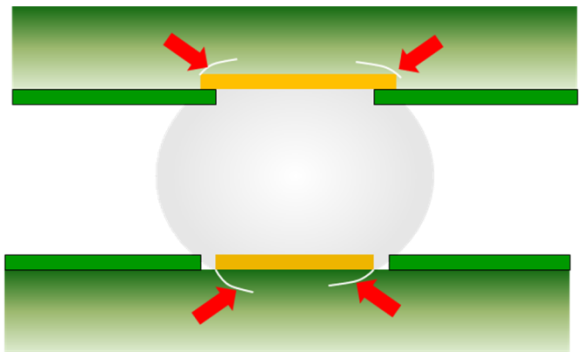

Figure 1 - Schematic Depiction of Pad Cratering

In recent years the industry has made significant advances in developing test methodologies to improve our understanding of pad cratering. A pad level pull test method has been developed to characterize the propensity of different laminate materials and pad designs [8]. This method has now been adopted as IPC standard 9708. However, in addition to pad level tests, board level tests are necessary to develop strain limits for PCBA level test and handling operations. For board level testing, the industry has traditionally relied on performing 4-point bend tests or spherical bend tests, and failure is often defined as the loss of electrical continuity in a daisy chain test vehicle [9, 10]. However in the case of pad cratering, this approach is flawed because the initiation of fine pad cratering cracks does not immediately disrupt the electrical continuity of a daisy chain net.

Electrical monitoring of daisy chain nets can only detect a very late stage of pad crater formation when the internal cracks have grown sufficiently large to cause an electrical trace to rupture. In order to circumvent this problem the present authors have recently developed and validated a novel approach which uses acoustic emission to detect the initiation of pad cratering failure [1, 2].

The acoustic emission (AE) approach is unique because it does not rely on an electrical signature to detect the onset of failure; instead elastic stress waves generated by the sudden initiation of pad cratering cracks are detected by piezoelectric sensors mounted on the test board. Our recent studies showed that by detecting AE events during 4-point bend tests we were able to accurately detect the initiation of both pad cratering and brittle intermetallic (IMC) fracture of solder joints [1, 2]. In addition to detecting the onset of failure, with the use of two AE sensors and prior knowledge of the velocity of sound in the PCB laminate, it was possible to accurately determine the location of failures which generated the AE events detected during bend tests. This methodology was validated by showing that the AE events detected during bend test were originating from the edges of the BGA package, which is where the first pad cratering failures would occur. In addition, physical failure analysis validated that solder joint cross-sections from samples without any AE activity did not have any pad cratering, while cross-sections of samples that generated AE events had clear evidence of pad cratering. Using this approach, we were able to determine the PCB strain limits for the initiation of pad cratering failures, and these strain limits were found to be significantly lower than those derived from electrical failure of the daisy chain nets. In this study, the AE method has been applied on a large body size flip-chip BGA (FCBGA) test vehicle to assess the strain limit for pad cratering. In a further extension of the AE methodology, four sensors have been used to determine the planar location of failures generated during four-point bend tests. The effects of design and process variables such as NSMD or SMD pad design, normal or diagonal strain orientation, and single or multiple reflow cycles have been investigated.

Test Vehicle

The tests were performed on daisy chain 40 x 40 mm FCBGA packages with organic built-up substrate and fully populated Sn-3.0%Ag-0.5%Cu (SAC305) solder balls with 1 mm pitch (Figure 2). The test board was designed to be double sided with the FCBGA assembled either on side A or side B. On side A, the FCBGA was oriented at a 0° angle as shown in Figure 3, while on side B the FCBGA was oriented at a 45° angle as shown in Figure 4.

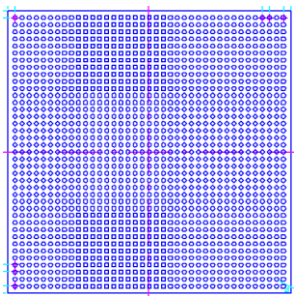

Figure 2 - FCBGA Footprint, 40 x 40 mm Body Size, 1mm Pitch

The 40 x 40 daisy chain package was tested with either 0° orientation, where the component edges were parallel to the board's edges or with 45° orientation where the component was at a 45° angle. The 0° board represents the case where the bending axis is normal to the edges of the component, while the 45° board represents the case where the bending axis is along the component diagonals. Arguably the 45° orientation may be more representative of actual handling operations in functional PCB assemblies. In addition to component orientation, the test boards were designed to have either a full array of non-solder mask defined (NSMD) pads, or solder mask defined (SMD) pads at only the six corner-most BGA pads at all four corners of the package. The pad diameter for NSMD PCB pads was the same as the mask opening of the BGA substrate. In the case of SMD pads at package corners, the pad diameter was slightly larger and the solder mask opening matched the mask opening of the BGA substrate. In order to simulate a functional PCB board design, it was desirable to have Plated Through-Hole (PTH) vias connected to all BGA pads. Since this was not possible at the pad locations where side A and side B of the BGA footprint overlapped, only the package corners were designed to be connected to PTH vias. Figure 5 shows the PCB pad layout near the package corners with SMD pads at the six corner-most locations. Note that the PTH vias were located inwards, towards the center of the package, in order to prevent PTH vias from shielding the solder joints during the bend tests.

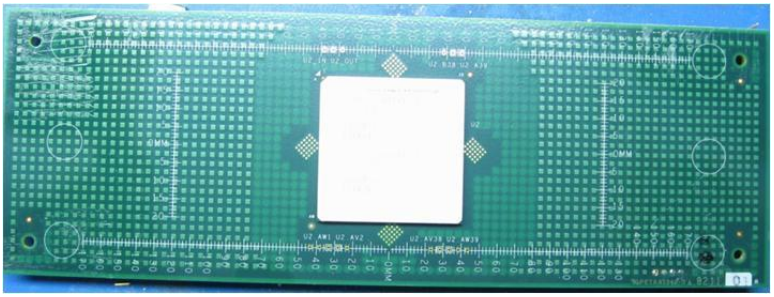

Figure 3 - Test Vehicle Side A, 0° Orientation

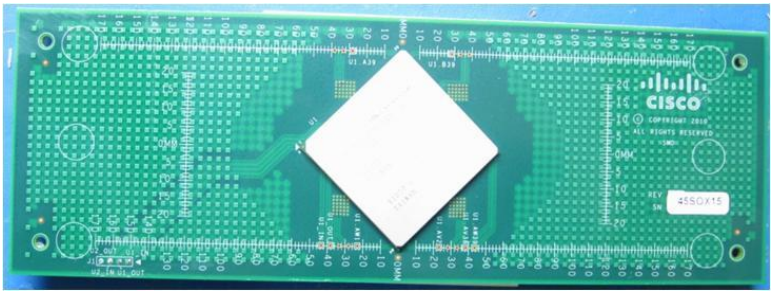

Figure 4 - Test Vehicle Side B, 45° Orientation

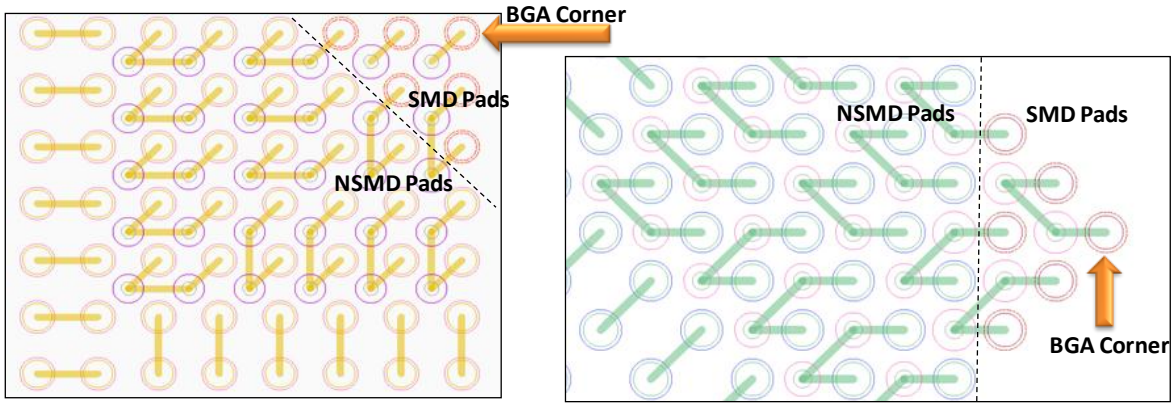

Figure 5 - PCB Pad Layout with SMD Pads at Package Corners

The test boards, assembled with components either on side A (0°) or side B (45°) were in some cases subjected to two additional reflow cycles (total 3X reflows) after board assembly. Our prior study showed that boards subjected to multiple reflows are more prone to pad cratering [2], therefore the case of 3X reflows was included in the present study to simulate a more realistic assembly process that could include two reflows from double sided board assembly and an additional reflow cycle from the wave soldering.

Test Procedure

Four point bend tests were performed according to IPC-9702 using daisy chain BGA test vehicles. Tests were carried out a strain rate of 5500 microstrain/second, in accordance with requirements of IPC-9702, because brittle intermetallic (IMC) fracture of solder joints is likely to occur only at high strain rate. Note that in our recent studies, it was demonstrated that pad cratering occurs at both slow and fast strain rates, but the strains required to generate pad cratering failure were lower at high strain rate [1, 2]. The bend test set-up is schematically shown in Figure 6. Details of the test matrix, including the variables considered in this study are shown in Table 1.

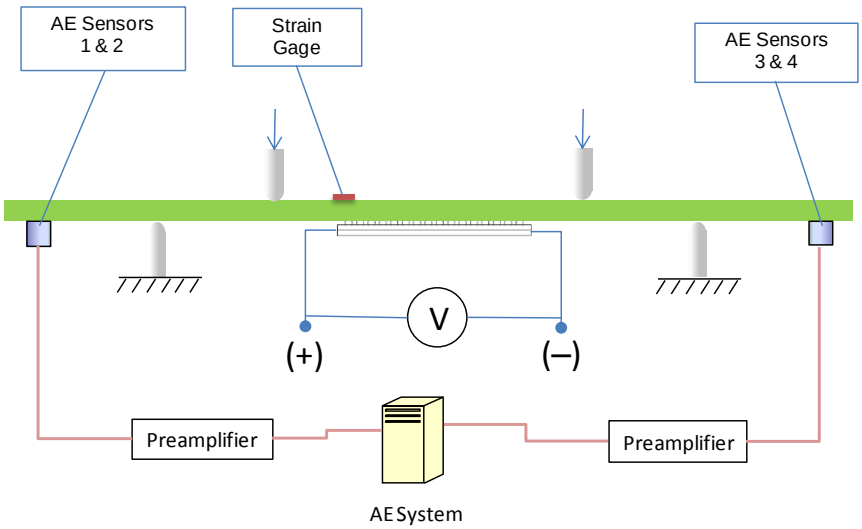

Figure 6 - Schematic of Bend Test Set-up with AE Sensors

Table 1 – Test Vehicle and Bend Test Details

Package	Ball Count	1521
	Pitch	1.0 mm
	Body Size	40 mm x 40 mm
	BGA Pad	0.48 mm SMD
	BGA Finish	Solder on Pad (SOP)
	Solder Composition	SAC305
	Solder Ball Diameter	0.6 mm
PCB	PCB Size	220 mm x 75 mm x 2.36 mm
	PCB Finish	OSP
	Laminate	Lead Free Compatible, T_g = 180°
	BGA Orientation	0° or 45°
	PCB stack-up / thickness	8-layer, 93 mil
	Pad Design	Full Array NSMD or 6 Corner SMD
	NSMD Pad Diameter and SMD Mask Opening Diameter	0.48 mm
Assembly	Number of Reflows	1X or 3X
Bend Test	Load Span	90 mm
	Support Span	140 mm
	Strain Rate	5500 microstrain/sec
	Number of AE Sensors	4

Four Acoustic Emission (AE) sensors were attached to the test boards to detect the AE events generated from pad cratering or BGA brittle fractures, and also to detect the location of the source of AE activity. In our previous work, two AE sensors were used to determine the linear location of AE events. In this study, with the use of four sensors the methodology was extended to determine the spatial location of AE events in the two-dimensional plane of the test board. These tests were done on assembled 0° and 45° boards, with a small load applied to ensure good contact between the anvils of the bend test fixture and the surface of the board. The algorithm for determining the location of an AE source relies on the velocity of sound in the PCB laminate and the time differential between detection of the same AE event at different sensors [1]. For this study, the orthotropic nature of the laminate was considered and different values were used for the velocity of sound (v_x *and* v_y), where X is the direction along the length of the board, and Y is along the width. Once the values of v_x and v_y were fine-tuned, a series of "pencil lead break" (PLB) tests were performed to calibrate the accuracy of AE source location. This is a simple procedure wherein the tip of a 0.5 mm mechanical pencil is broken on the board, at a approximately 60° angle from the surface of the board, in order to simulate at AE event. Since the position of the PLB test in known in advance, the location of the event detected by the AE system provides a means to evaluate, and iteratively improve, the accuracy of the source location. Figure 7 shows the AE source location result from a 0° board after pencil lead breaks at the package center, package corners, and near the loading anvils of the fixture.

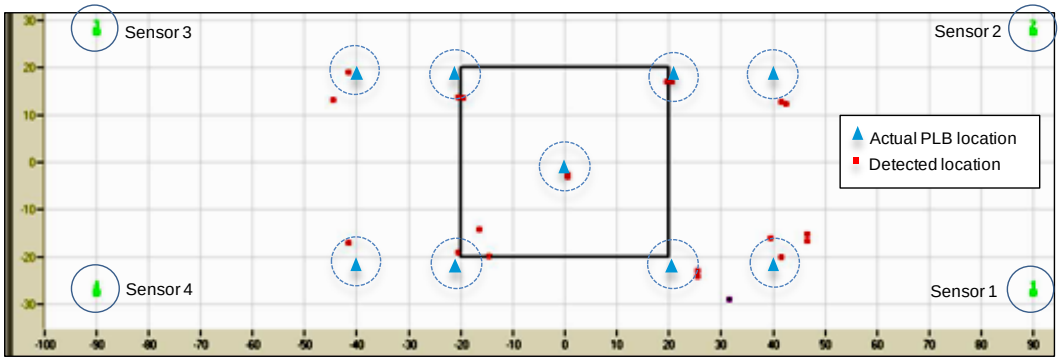

Figure 7 - Pencil Lead Break Result with 0° Orientation

By comparing the location of the actual PLBs and the detected position of AE events, it is estimated that the source location accuracy is approximately 5 mm near the center and edges of the FCBGA, and approximately 7 mm near the fixture anvils. The ability to detect the location of AE events significantly enhances the test methodology by not only detecting the onset of AE activity but also being able to validate that the source of this activity was located near the edges of the package where the first pad cratering or brittle solder joint failures would be expected.

During the actual bend tests, in addition to AE sensors, a single axis strain gage was attached on the secondary side directly beneath a corner BGA pad. This strain gage provided the maximum strain along the length of the board. A D.C. power supply was also connected to the terminals of the daisy chain package in order to monitor the electrical continuity of the daisy chain. This was done indirectly by monitoring the voltage under constant current. An integrated data acquisition system recorded the load, displacement, AE activity from four sensors, strain, and voltage of the daisy chain circuit during the tests. Additional details of the test approach may be found in our previous study [1].

Test Results

Figures 8 and 9 show the typical data acquired during the FCBGA bend tests. For a 45° sample, Figure 8 (a) shows the AE events acquired over time as a function of the detected X and Y coordinates of the AE source. The edges of the FCBGA package have been indicated for convenience. Figure 8 (b) shows the same result in a two-dimensional graph of the Y coordinate versus X coordinate of the detected AE event. Note that these detected locations are approximate since the accuracy of AE source location was estimated to be approximately 5 mm from the PLB tests. With this limitation in mind, it is interesting to note that the AE events were clearly concentrated near the left and right corners of the package. These are the locations where the first failures would be expected during four-point bend tests. Similarly, in samples with 0° orientation, the failures were clustered along the left and right edge of the package where the first failures are expected to occur. Figure 9 shows the displacement and daisy chain resistance data acquired for the same sample used as an example in Figure 8. It was found that after the start of the bend test, there was a well defined period of time, annotated as the “Quiet Zone”, during which there was no AE activity. Once the first AE activity began, several consecutive AE events were detected. Most of these early events were clustered at the package corners. Figure 9 shows that the resistance of the daisy chain net was not affected during most of the early AE activity. It was only in a very late stage of the test when the electrical resistance indicated at open circuit. Note that in many cases, the resistance of the daisy chain was not affected even after the bend test was completed. In cases where electrical failure was detected, the onset of AE activity always preceded electrical failure. This result was typical for both 45° and 0° boards.

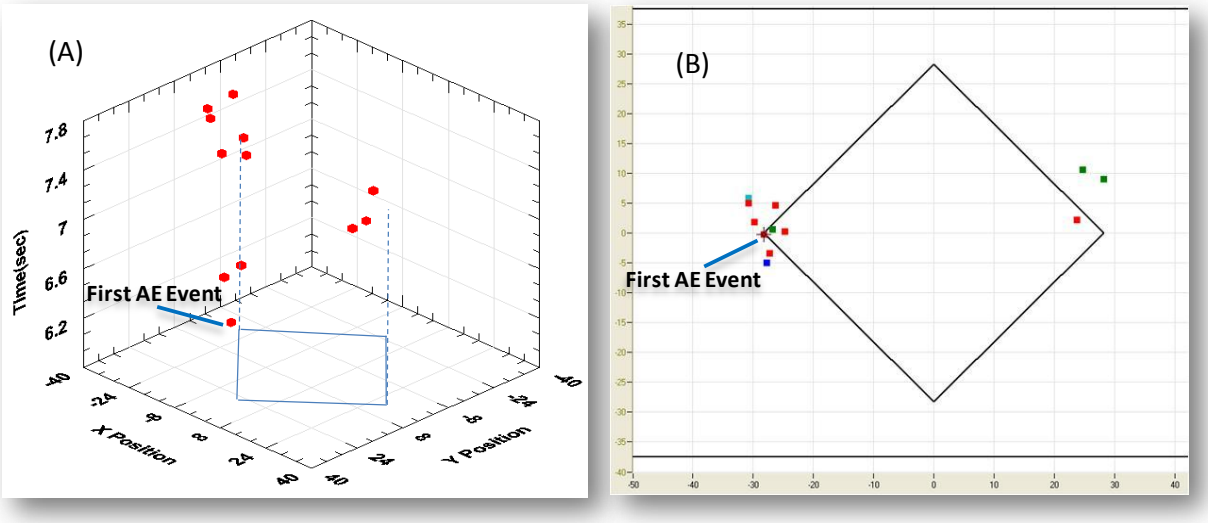

Figure 8 - AE Source Location during Bend Test with 45° BGA Orientation

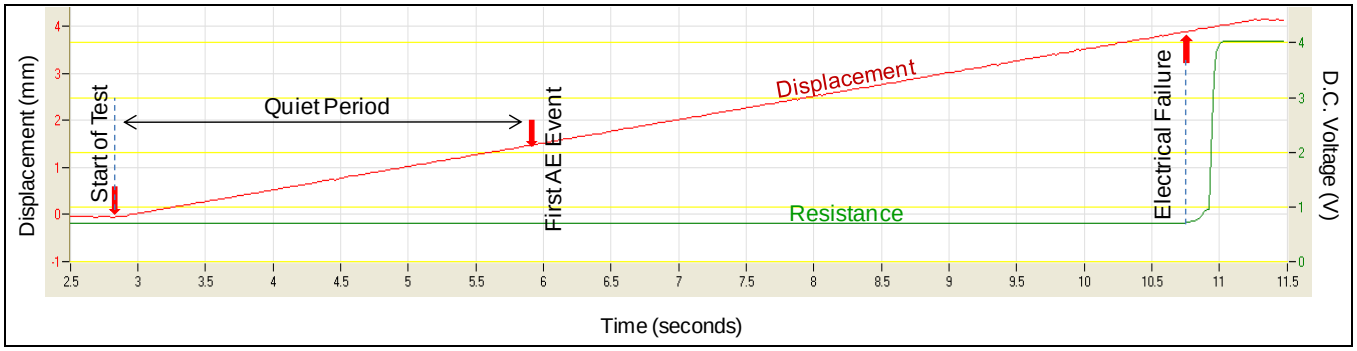

Figure 9 - Acquired Displacement and Resistance during Bend Test with 45° Orientation

Following the bend tests, cross-sections and dye-and-pry were performed to determine the failure modes. The samples with 0° BGA orientation were cross-sectioned along the edges (parallel to the fixture anvils). The samples with 45° orientation were cross-sectioned diagonally along the direction perpendicular to the fixture anvils. In order to validate the effectiveness of the acoustic methodology, a few bend tests were terminated before any AE events were detected. Some bend tests were terminated after AE events were detected, and in most cases the tests were terminated after electrical failure. Figure 10 shows typical cross-section results after various stages of bend testing. If no AE event was detected, cross-sections did not show any signs of failure. This result was critical for validating the AE test methodology and similar validation was performed in our previous work on different types of components [1]. Also shown in figure 10 are cross-sections of samples where tests were terminated after AE event detection, but before electrical failure. The failure modes were found to depend on the PCB pad design. In the case of full array NSMD pads, the failures were always due to pad cratering on the PCB side. In the case of boards with corner SMD pads, there were three different failure modes. The solder joints with corner SMD pads had partial IMC fracture at either the BGA package side or PCB side. In some cases the joints with partial IMC fracture also showed partial PCB pad cratering. This result clearly demonstrates that the AE methodology is an effective tool for detecting the onset of different failure modes, i.e., BGA side IMC fracture, PCB side IMC fracture, or pad cratering. As seen in figure 10, the partial nature of the IMC fractures explains why these failures did not result in instantaneous electrical failure of the daisy chain circuit. In samples cross-sectioned after electrical failure, the same failure modes had progressed to a greater extent. The IMC fractures of joints with corner SMD pads showed complete separation along the joint diameter, and PCB side pad cratering showed a larger extent of cracking which may have ultimately ruptured a trace in the daisy chain circuit.

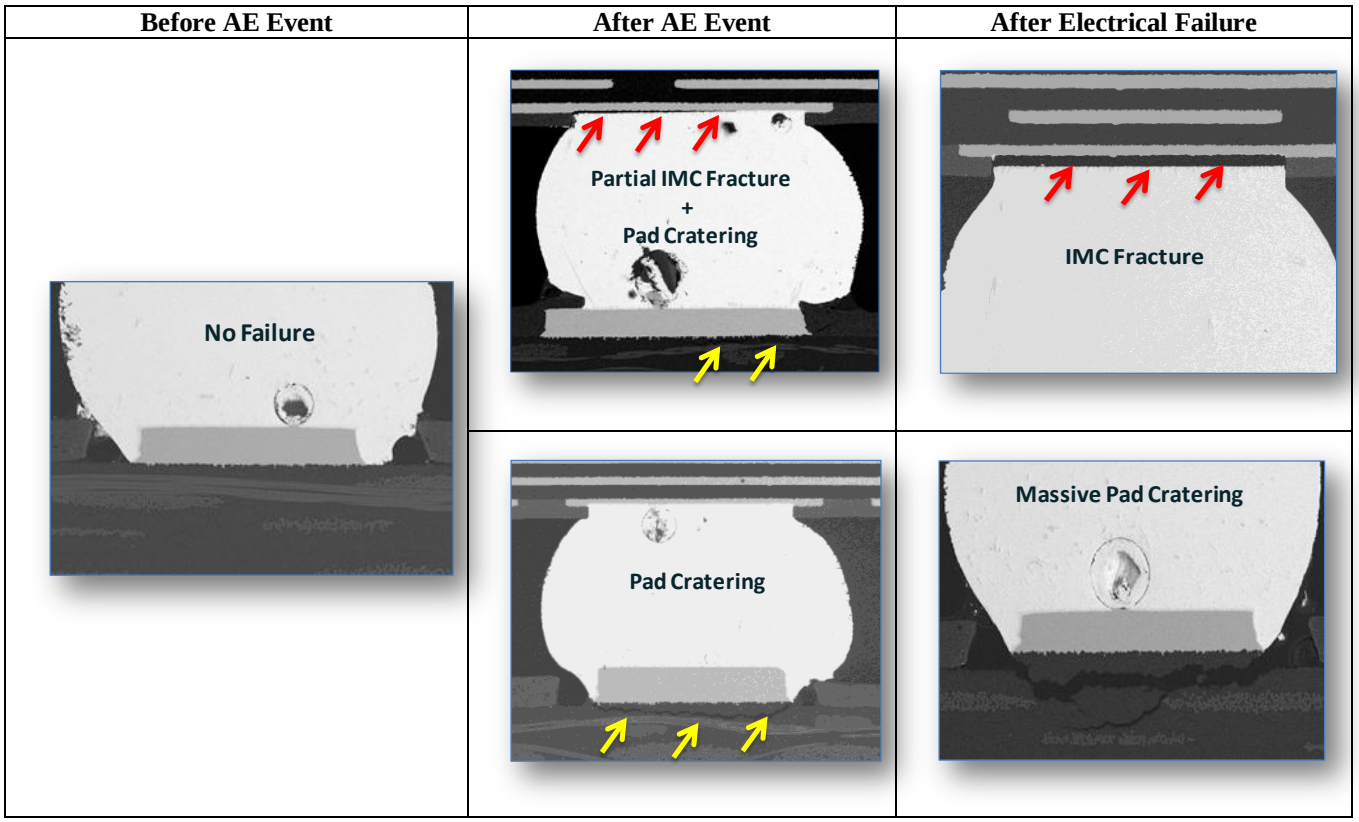

Figure 10 - Typical BGA Cross-sections with Full NSMD and Corner SMD Pads

The dye and pry tests showed the same failures modes observed by cross-sections. Dye and pry images and a schematic mapping of failures modes are shown in figure 11. As expected, the area of solder joint failures was strongly impacted by the component orientation. In 0° samples the damage was along the left and right edges, whereas in 45° samples the damage was along diagonally opposite corners of the package. The failure mode was completely dependent on the PCB pad geometry. With NSMD pads the failures were always due to pad cratering in the PCB laminate. In the case of corner SMD pads at the PCB corners, the failure mode shifted to IMC fracture at either the PCB side or the BGA substrate side (Figure 12). It is interesting to note that within the samples with corner SMD pads, the predominant failure mode in the remaining solder joints with NSMD pads was still PCB side pad cratering.

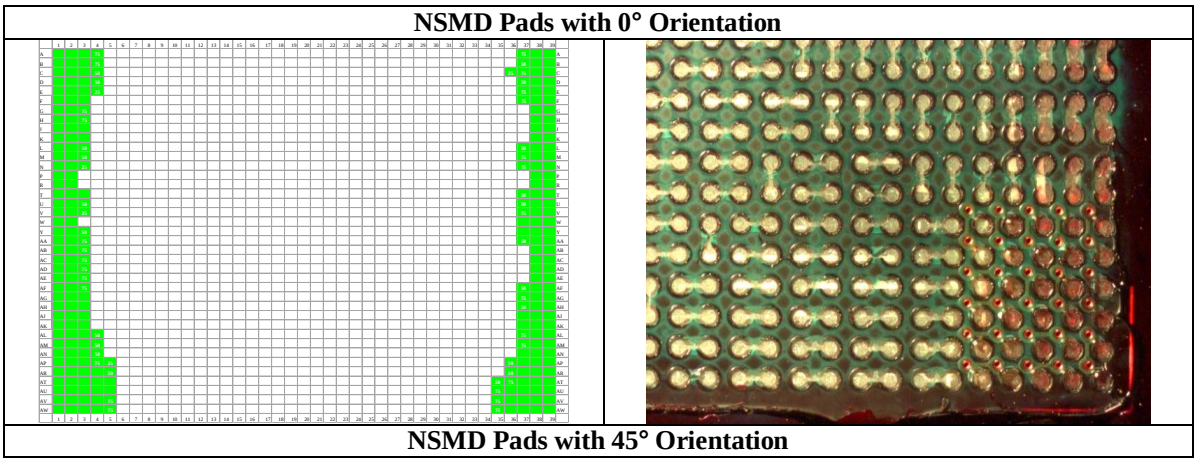

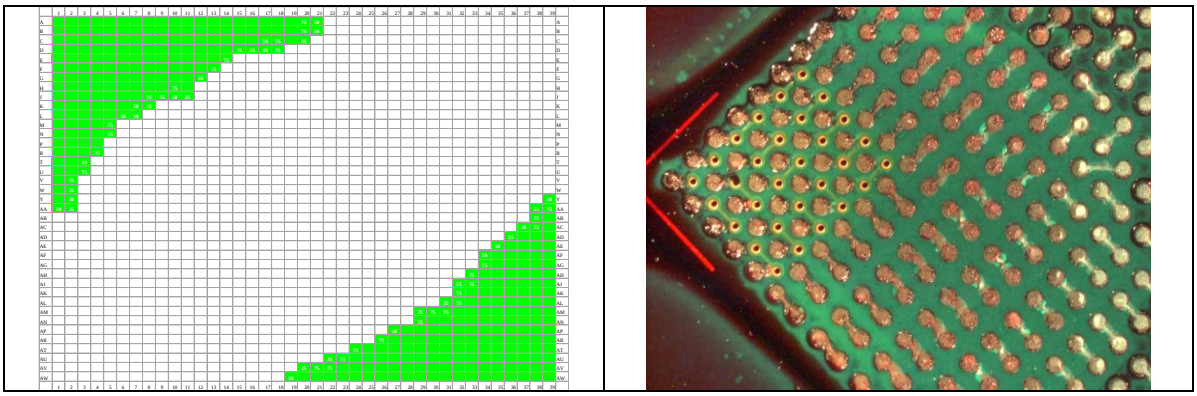

Figure 11 - Typical Dye and Pry Result with Full NSMD Pads (Green - PCB Pad Cratering)

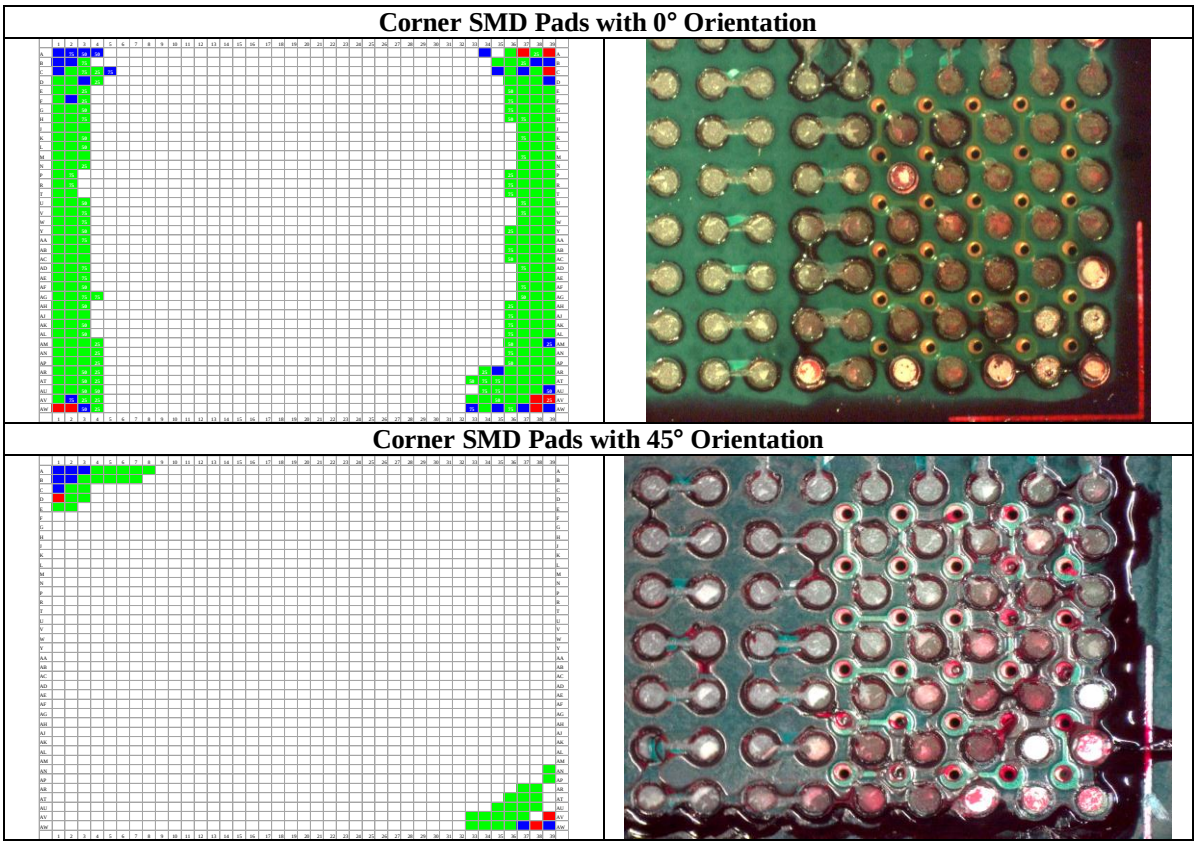

Figure 12 - Typical Dye and Pry Result with Full NSMD Pads (Blue – BGA Side IMC Fracture, Red – PCB Side IMC Fracture, Green - PCB Pad Cratering)

Having characterized the failure modes, we can now review the effects of design and process variables on the onset of failures in the FCBGA test vehicle. The single axis strain gage mounted on the secondary side of the board, directly beneath a corner-most BGA pad, was used to determine the PCB strain. Figure 13 shows the failure strains for the full matrix of tests conducted in this study. The failure strains showing the onset of both AE failure and electrical failure can now be used to perform a detailed investigation of the effects of component orientation, number of reflow cycles, and PCB pad design. Note that in several cases, the maximum banding strain applied during the tests was not sufficient to generate electrical failures. In order to account for these "survivors", the maximum bending strain has been shown as the electrical failure strain in figure 13. In most samples, AE failure was detected before electrical failure and in a few samples the AE failure and electrical failure occurred simultaneously. In comparison with the splits with corner SMD pads, the strain gap between AE failure and electrical failure was significantly larger for the splits with a full array of NSMD pads.

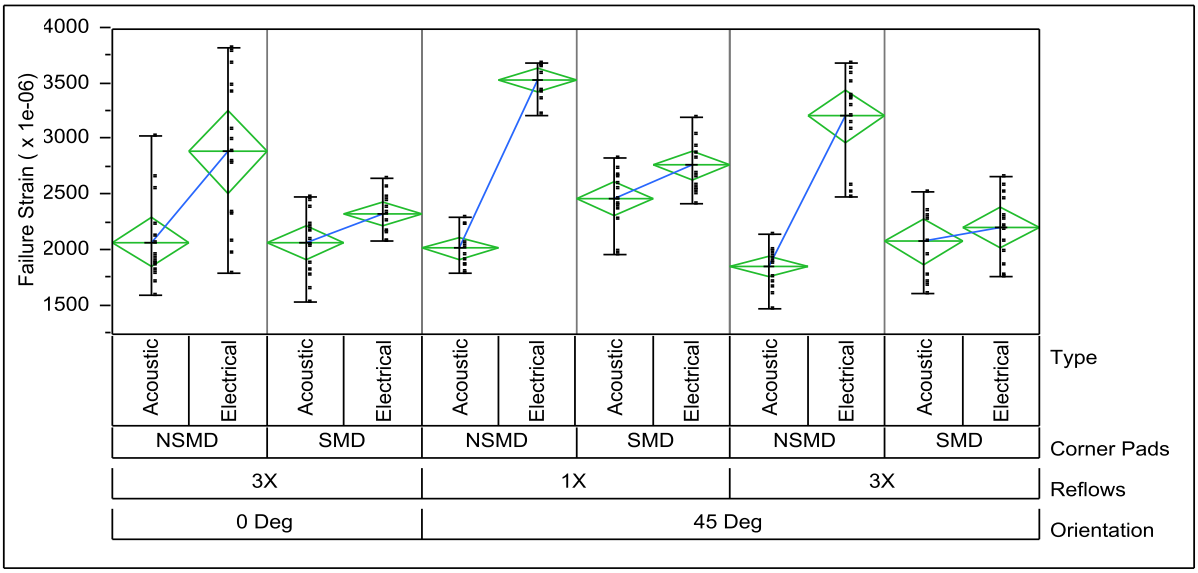

Figure 13 – AE and Electrical Failure Strain from all Test Splits

Discussion

While the results from all splits in the test matrix are shown in figure 13, a detailed examination of the effects of individual variables and their interactions is performed in this section. Note that this analysis will consider only AE failures since AE represents the initiation of failure, while electrical failure of the daisy chain occurs at higher strain under monotonic bending.

(i) Effect of Component or Strain Orientation

The 0° and 45° orientation of the component may be considered synonymous with variation in the direction of the bending strain; therefore this parameter may also be referred to as the strain orientation effect. From a practical viewpoint, the 45° strain orientation is perhaps more relevant because most actual assembly and test operations will tend to apply bending strains along the diagonal. Figure 14(a) shows a comparison of AE failure strains for 0° and 45° samples with NSMD and corner SMD PCB pads. All samples in this case were subjected to 3X reflow prior to bending. Figure 14(b) shows the interaction of mean AE failure strain with PCB pad type. In the case of corner SMD pads, it is clear that the component or strain orientation had a negligible impact. However, in the case of NSMD pads where the failure mode was PCB pad cratering, the 45° orientation had lower failure strains than the 0° orientation. This implies that the propensity for pad cratering is higher if bending strain is applied along the component diagonal. Another interesting observation is that in the case of 0° orientation the effect of corner pad design was negligible.

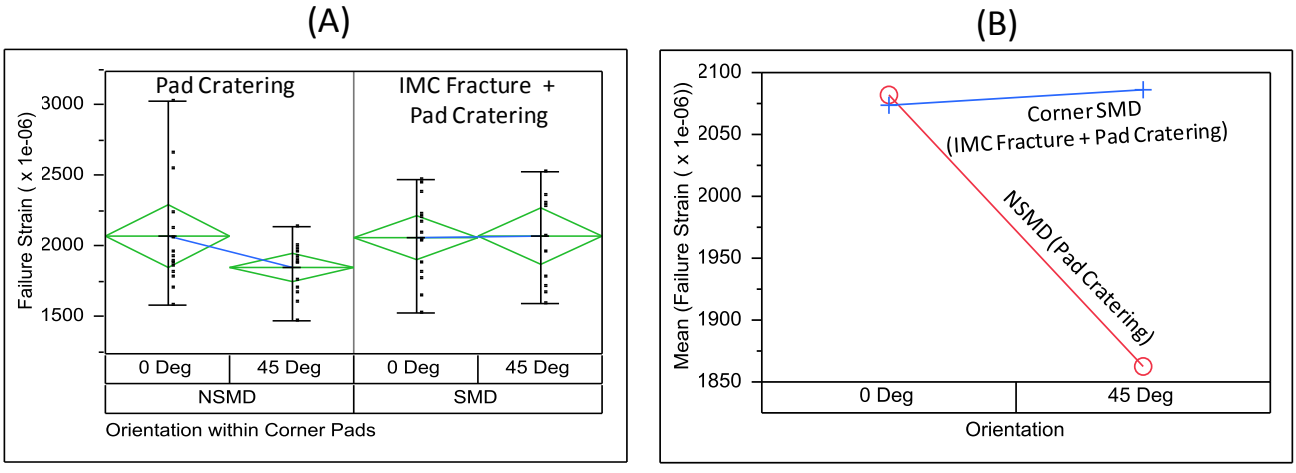

Figure 14 - AE Failure Strain Comparison showing Effect of Pad Design and Orientation

(ii) Effect of Number of Reflows

Figure 15(a) shows a comparison of the failure strains with NSMD and corner SMD PCB pads tested after a single reflow cycle and after a total of 3X reflows. These results are from samples with 45° orientation only. Figure 15(b) shows the interaction of mean failure strain with PCB pad design. With both NSMD pads and corner SMD pads, it is clear that the AE failure strain is reduced if the boards are preconditioned with multiple reflow cycles. For the case of NSMD pads, this finding is consistent with our prior observation on two different test vehicles [1, 2]. As pad cratering was the only failure mode in this case, it is clear that multiple reflow cycles are detrimental for PCB pad cratering. Since actual assembly of a complex double sided board will involve at least 2X reflow, and often 3X reflow if wave soldering or rework are involved, it is highly recommended that test samples to characterize pad cratering be subjected to 3X reflow preconditioning. In the case of corner SMD pads where the failure mode involved IMC brittle fracture and PCB pad cratering, the results show that the additional copper consumption and growth of the IMC layers associated with multiple reflows will be detrimental for the brittle fracture strength of the solder joint. A detailed microstructural analysis of the effect of multiple reflows is beyond the scope of this study.

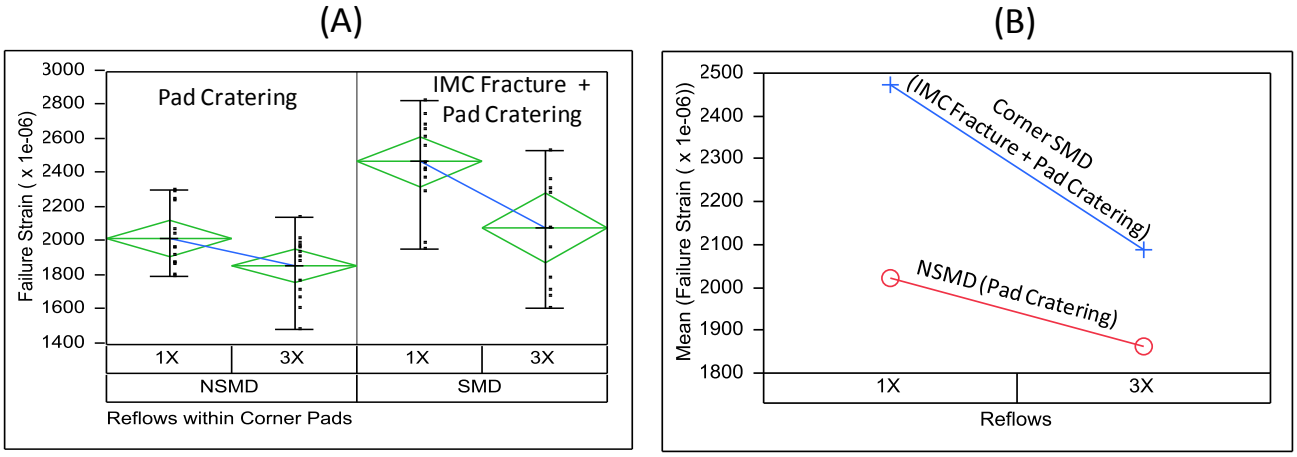

Figure 15 - AE Failure Strain Comparison showing Effect of Pad Design and Number of Reflows

(iii) Effect of Corner PCB Pad Design

From the results shown so far, it is clear that the design of the corner PCB pads had a significant impact on the failure mode and the failure strains based on both acoustic and electrical event detection. With a full array of NSMD PCB pads, the failure mode was PCB pad cratering and the electrical failure strain was significantly higher than the AE failure strain (Figure 13). In contrast, with the use of corner SMD pads, the failure mode was a combination of package or PCB side IMC fracture and pad cratering, and the electrical failure strains were significantly lower. In these cases, the strain gap between AE failure and electrical failure is significantly reduced. With a full array if NSMD pads, figures 14 and 15 show that the mean AE failure strain is significantly reduced with the 45° orientation and after 3X reflows. This is a clear indication that the risk for pad cratering is higher if bending strain is aligned with the component diagonal and after multiple reflows. In contrast with corner SMD pads, there was no effect of orientation, but multiple reflows reduced the failure strain for the mixed failure mode of IMC fracture and pad cratering.

As noted in the introduction, the lack of a suitable board level test methodology to detect the onset of pad cratering has been a significant barrier for determining the PCB strain limits. The failure strains based on electrical resistance monitoring will significantly overestimate pad cratering resistance, and should therefore not be used to determine strain limits for actual PCB assembly, test, and handling operations. With use of the AE method, we can now see that the failures are initiating at significantly lower strain levels and by fitting an appropriate distribution it should be possible to establish the true strain limits. The AE failure data were fitted with a 2-parameter Weibull distribution for the cases of NSMD and corner SMD pads, with 0° and 45° orientations after 3X reflow preconditioning (Figure 16). Using a failure rate of 1%, the PCB strain limits were found be in the range of 1250 to 1350 microstrain, i.e. very similar for all cases except the case of corner SMD pads with 45° orientation. In this case the strain limit was approximately 850 microstrain. The significantly different behavior of this case is not apparent in comparison of the mean failure strains due to a lower slope. Since the slope of the Weibull fit is often an indicator of the failure mode in reliability tests, it may be speculated that while mixed failure modes were observed with corner SMD pads, it appears that pad cratering was the dominant failure mode with the 0° orientation and IMC brittle fracture was the dominant failure mode with 45° orientation.

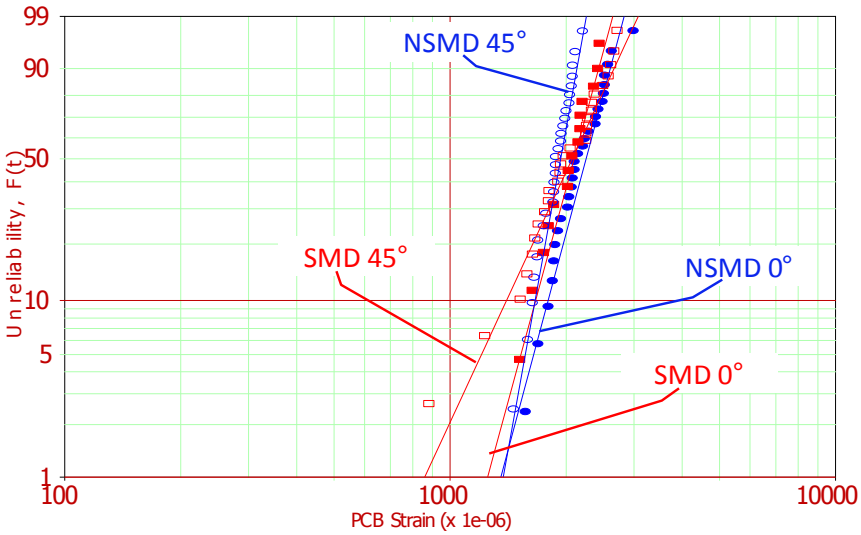

Figure 16 - Weibull Distribution of AE Failures

In our prior study, a similar body size wire bonded HSBGA package was subjected to these tests and the PCB strain limit was found to be significantly higher than the stiffer FCBGA package evaluated in this study. This shows that in addition to package size and BGA pitch, the stiffness of the package has a significant impact on the strain limits.

Conclusions

Results from this study demonstrated that monitoring Acoustic Emission during board bending tests is an effective methodology to detect the initiation of pad cratering and partial brittle IMC cracks at the BGA joints. While the utility of the AE method was previously demonstrated to detect pad cratering [1, 2], this study shows that even brittle fracture at the IMC layers may be partial in nature and may not cause instantaneous electrical failure. The conventional approach of using electrical tests will therefore significantly overestimate PCB bending strain limits for board handling and test operations. Using the AE method, the mechanical bending strain limit was determined for a 40 x 40 mm FCBGA package with a full array of NSMD pads and SMD pads at the corners. The effects of PCB pad design, component orientation, and number of reflows were investigated in detail. The failure mode was highly dependent on the PCB pad design. With a full array of NSMD pads only pad cratering failures were observed. With the use of corner SMD pads, the failure mode shifted to a combination of brittle IMC fracture and pad cratering. In contrast with full NSMD pads, the use of corner SMD pads resulted in significantly lower electrical failure strains. Tests with 0° and 45° component/strain orientations, tested after 1X or 3X reflows, showed that the propensity for pad cratering is higher if the bending strain is oriented along the component diagonal and if the boards are subjected to multiple reflow cycles. The propensity for brittle IMC fracture is also higher after multiple reflows, but the effect of strain orientation was insignificant.

Acknowledgements

The authors wish to thank Gnyaneshwar Ramakrishna of Cisco Systems, Inc. for his valuable suggestions. Thanks are also due to Mason Hu of Cisco Systems, Inc. for supporting this project.

References

[1] A. Bansal et al, “A New Approach for Early Detection of PCB Pad Cratering Failures”, IPC/APEX Conference, Las Vegas, NV, April (2011)

[2] A. Bansal et al, “Method for Early Detection of PCB Bending Induced Pad Cratering”, Engineering Components and Technology Conference (ECTC), Lake Buena Vista, FL, June (2011)

[3] G. Godbole et al, “On The Nature of Pad Cratering”, Proc. 59th Electronic Components and Technology Conference (ECTC), (2009)

[4] G. Long et al, “Lead Free Assembly Impacts on Laminate Material Properties and “Pad Crater” Failures”, IPC APEX Conference, (2007)

[5] B. Gray et al, “Mechanical Failures in Pb-free Processing: Selected Mitigation Techniques for Pad Crater Defects”, SMTA Intl. Conference, (2010)

[6] D. Xie et al, “Failure Mechanism and Mitigation of PCB Pad Cratering”, Electronic Components and Technology Conference (ECTC), (2010)

[7] H. Ma et al, “Acceleration Factor Study of Lead-Free Solder Joints under Wide Range Thermal Cycling Conditions”, Electronic Components and Technology Conference (ECTC), (2010)

[8] M. Ahmad et al, "Validated Test Method To Characterize And Quantify Pad Cratering Under BGA Pads On Printed Circuit Boards", IPC/APEX 2009 Conference, Las Vegas, NV, April, (2009)
[9] IPC/JEDEC 9702, Monotonic Bend Characterization of Board Level Interconnects
[10] IPC/JEDEC-9707, Spherical Bend Test Method for Characterization of Board Level Interconnects